Experimental and numerical studies on shear behaviour of macro-synthetic fibre reinforced prestressed concrete beams

Lakavath, Chandrashekhar; Suriya Prakash, S.; Dirar, Samir

DOI:
10.1016/j.conbuildmat.2021.123313

Document Version
Peer reviewed version

Citation for published version (Harvard):
Lakavath, C, Suriya Prakash, S & Dirar, S 2021, 'Experimental and numerical studies on shear behaviour of macro-synthetic fibre reinforced prestressed concrete beams', *Construction and Building Materials*, vol. 291, 123313. https://doi.org/10.1016/j.conbuildmat.2021.123313

EXPERIMENTAL AND NUMERICAL STUDIES ON SHEAR BEHAVIOUR OF MACRO-SYNTHETIC FIBRE REINFORCED PRESTRESSED CONCRETE BEAMS

Chandrashekhar Lakavath[1], S Suriya Prakash[2] and Samir Dirar[3]

[1]Research Scholar, Email: ce19resch11007@iith.ac.in
[2]Professor and Corresponding Author, Email: suriyap@ce.iith.ac.in
[3]Associate Professor, Email: s.m.o.h.dirar@bham.ac.uk
[1,2]Civil Engineering Department, Indian Institute of Technology Hyderabad, India, 502 285.
[3]Civil Engineering Department, University of Birmingham, Birmingham B15 2TT, UK.

ABSTRACT

Experimental and numerical studies on shear behaviour of macro synthetic fibre reinforced prestressed concrete (MSFRPC) beams are presented. MSFRPC beams are tested at a shear span to depth ratio (a/d) of 2.4 to understand the role of macro synthetic polyolefin fibres on the shear resistance and failure modes. The fibre volume fraction of 0.0%, 0.5%, 1.0% and 1.5% are considered as study parameters. A three-dimensional nonlinear finite element (FE) analysis is carried out to understand the influence of fibres on shear behaviour using the concrete damage plasticity model. Tensile constitutive relations of FRC is derived using inverse analysis from fracture test results and used as input in the FE model. A stage-wise analysis is conducted to include the effects of prestressing and applied external shear loads. The results from FE analysis showed a good agreement with experimental results for different fibre dosages. The effect of level of prestressing and varying compressive strength is studied through calibrated FE models. Due to the addition of macro synthetic fibres, no significant improvement in compressive strength is observed. Low fibre volume addition of 0.5% did not produce an appreciable improvement in shear behaviour. However, test and FE results of beams with higher volume fractions of 1.0% and 1.5% significantly improved the post-cracking behaviour, ductility, and ultimate shear resistance of MSFRPC beams.

Keywords: ABAQUS, Concrete damage plasticity, DIC, Shear, Prestressed concrete beams, Polyolefin fibres.

1.0 INTRODUCTION

High-strength prestressed concrete (PC) beams are commonly used in various prestressing applications [1–3]. Though the use of high-strength concrete has several advantages, it increases the brittle behaviour of PC members. PC beams can fail in a brittle manner under shear dominant loading [1,2,4–6]. The shear behaviour and failure modes of the PC beam depends on various parameters such as compressive strength of concrete, longitudinal and shear reinforcement ratio, level of prestressing, and level of flexure to the shear stress ratio at the critical section. This study tries to understand the shear behaviour of macro-synthetic fibre reinforced prestressed concrete (MSFRPC) beams. Adding discrete fibres in concrete can ensure adequate ductility of prestressed concrete members under various loading conditions.

The use of fibre-reinforced concrete (FRC) in prestressing application can improve the ductile performance by preventing crack progression. Previous studies on FRC highlighted the beneficial effects of fibres on improving the performance of concrete at both the material and member level [7–15]. ACI provisions [16] suggest a minimum of 0.75% of the volume fraction of steel fibres for replacing the stirrups [15,17]. Lakavath et al. [18] previously investigated the influence of steel and hybrid fibres on the shear behaviour of prestressed concrete beams. A significant improvement in shear capacity was observed due to the addition of 0.5% and 1.0% volume fraction of steel fibres. While the remarkable mechanical performance of steel fibre addition to concrete is recognized, such a combination has durability issues. Steel is not only highly corrodible but also costly to purchase, store and handle. Durability issues associated with SFRC have forced the manufacturers and engineers to develop a variety of fibres with specific properties for construction-related applications. Synthetic fibres such as polyolefin-based macro-synthetic fibre

types can solve the issues of reduced workability of FRC and corrosion without significantly compromising the structural performance. Studies in the past [19–25] have showcased that synthetic fibre reinforced concrete (SynFRC) is cost-effective in improving the tensile behaviour of concrete.

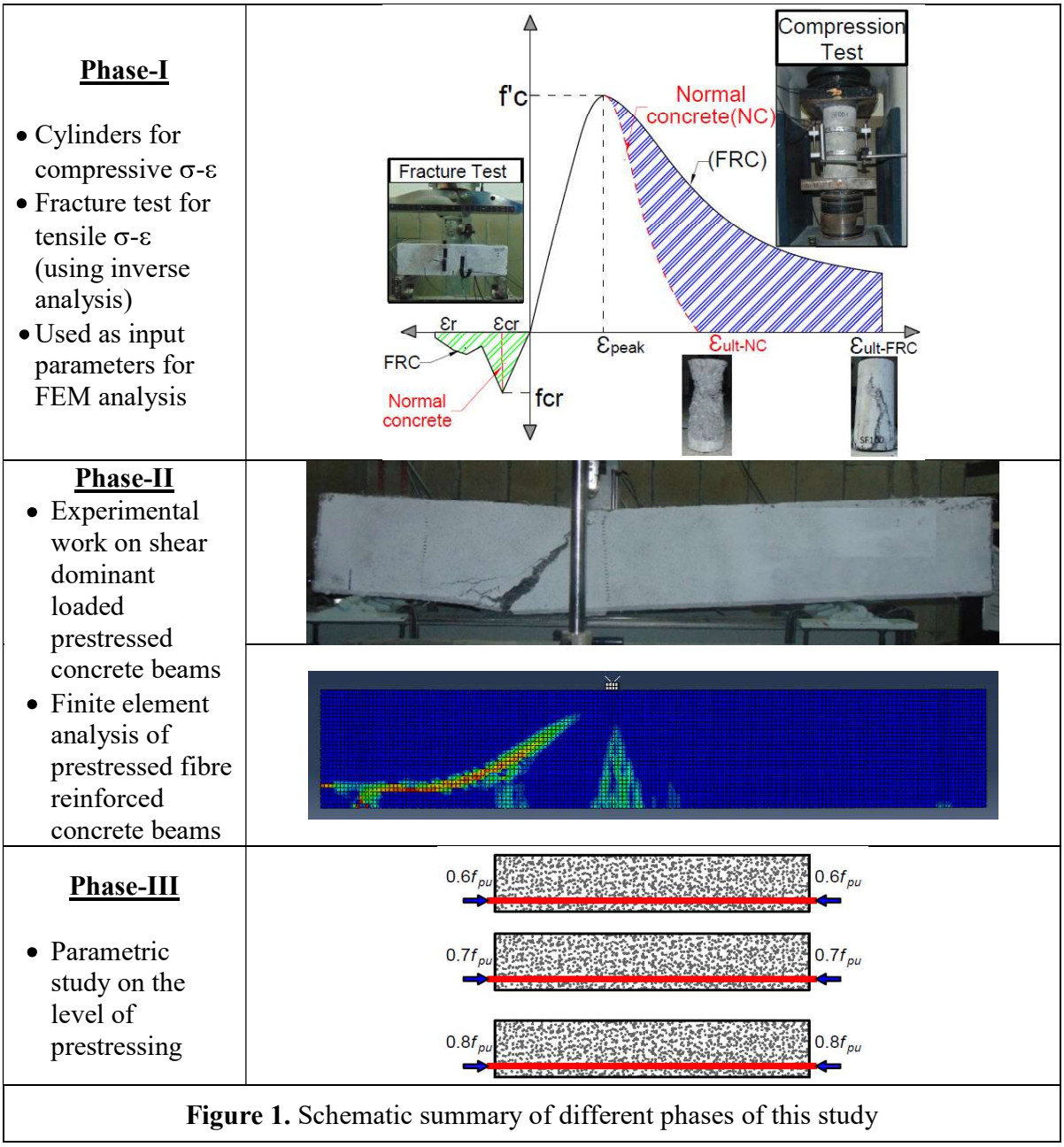

Figure 1. Schematic summary of different phases of this study

Only a few authors in the past have focused on modifications of plasticity-based constitutive models [26]. The existing continuum plasticity damage model [27,28], such as the concrete damage plasticity (CDP) model, is used in this study. Only a few researchers in the past have used calibrated tensile constitutive behaviour of FRC in FEM simulations through inverse analysis [29]. The schematic presentation of different phases involved in this study is shown in **Figure 1**. Phase-I includes the material characterization of FRC in compression and tension. Phase-II consists of experimental studies on prestressed concrete beams with different fibre dosages at shear span to depth ratio of 2.4 and validation with finite element analysis. Finally, Phase-III includes parametric studies.

2.0 RESEARCH SIGNIFICANCE

Only minimal information exists on the behaviour of macro synthetic fibre-reinforced prestressed concrete beams subjected to shear dominant loads. Thus, macro-synthetic fibres reinforced prestressed concrete beams are tested under shear dominant loading (a/d=2.4 to fill the existing knowledge gap. Besides, fracture tests are conducted as well to understand the role of fibres in crack arresting. The main parameter considered in this study are different volume fraction of fibres such as (V_f = 0.0%, 0.5%, 1.0% and 1.5%). However, all other parameters such as compressive strength, dimensions of beam, and shear span to depth ratio are kept constant. The key observations due to the addition of fibres include variations in ductility, toughness, failure mode, and capacity of beams. Hence, the specific objectives of the present study are:

1. To understand the effectiveness of macro-synthetic fibres in improving the shear behaviour of prestressed concrete beams by carrying out experimental studies.

2. To monitor the crack initiation and its propagation in notched prism beams and full-scale prestressed concrete beams using digital image correlation technique (DIC).
3. To utilize the multi-linear stress-strain model (based on fracture tests) as an input for the nonlinear finite element analysis to simulate the shear behaviour of MSFRPC beams.
4. To carry out parametric studies on the influence of level of prestressing force on the shear behaviour of MSFRPC beams.

3.0 EXPERIMENTAL PROGRAM

Pretensioned beams of dimensions 150 mm x 300 mm x 1600 mm were cast in the precast factory and tested in heavy structures lab at the Indian Institute of Technology Hyderabad. Eight beams were tested at a shear span to depth (a/d) ratio of 2.4. As per Kani's classical theory [30], the *a/d* ratio of 2.5 is the transition point below which the RC beams fail in a shear critical mode. Therefore, *a/d* ratio of 2.4 is considered in this study to avoid arch action and ensure diagonal shear tension (DST) mode [31,32]. The variables considered in this study are 0.0%, 0.5%, 1.0% and 1.5% of volume fraction (V_f) of macro-synthetic fibres (MSF). In this study, MSF100 represents prestressed concrete beams reinforced with macro synthetic fibres of 1.0% by concrete volume. The concrete mix was designed to attain a strength of 50 MPa as per the Indian standard IS 10262 [33]. The design concrete mix includes the fine aggregates, coarse aggregate, cement, superplasticizer, and water content as detailed in **Table 1.** All the materials were added in the following sequence to avoid the balling effect. Firstly, the total quantity of coarse aggregates, fine aggregates, and cement was added, followed by 50% of the total water quantity. Afterwards, macro synthetic fibres were added manually, as shown in **Figure 2(b).** Finally, the remaining water and superplasticizers were added to the pan mixture. Details of fibre and manual addition of fibres to

the concrete while mixing is shown in **Figure 2**. The obtained target cube compressive strength is 58 MPa. In the same mix, the fibre volume of 0.5% (4.55 kg/m^3), 1.0% (9.1 kg/m^3) and 1.5% (13.65 kg/m^3) were added. The compressive strength of concrete cubes are 59 MPa, 67 MPa and 68 MPa, respectively. The properties of the macro-synthetic fibres in this study are shown in **Table 2**.

(a) (b)

Figure 2. Macro synthetic fibers (MSF) (a) Geometry (b) Mixing of MSF to concrete

Table 1. Concrete mix proportion in kg/m^3

Cement	CSS	NRS	Coarse aggregate		SP	Water	Macro-synthetic fibre (MSF) (V_f= 0%, 0.5%, 1.0% and 1.5%)
			20 mm	10 mm			
450	415	312	755	355	2.6	152	0.0, 4.55, 9.1 and 13.65

Note: CSS= Crushed stone sand, NRS= Natural River Sand, SP= Super Plasticizer

Table 2. Properties of macro-synthetic fibre (Polyolefin fibres)

Specification	Macro-synthetic fibre (MSF)
Specific gravity	0.91
Length (mm)	50
Diameter (mm)	0.5
Tensile strength (MPa)	618
Modulus of elasticity (GPa)	10
Aspect ratio	100

3.1 Compression Tests on Concrete Cylinders

Concrete cylinders of size 150 mm (diameter) x 300 mm (length) were tested under uniaxial compression to understand the effect of macro synthetic fibres in improving the strength and ductility. All the cylinders were tested in displacement control mode with a rate of 1 mm/min, using a servo-controlled compression testing machine of 500 kN capacity. Three linear variable displacement transducers (LVDT) are attached to cylinders for monitoring the axial deformation. Average compressive stress-strain curves are shown in **Figure 3**. Test results revealed that the addition of fibres does not significantly influence the cylinder compressive strength. However, the compressive toughness index increased from 1.4 to 5.7 times due to the addition of macro synthetic fibres **(Table 3).** The toughness of MSF50 increased by 40% when compared to control cylinders due to the addition of 0.5% fibre volume dosage. However, the ultimate strain of MSF50 did not increase as that of MSF100 and MSF150 (**Figure 3)**. In MSF50 specimens, the crack bridging and passive confinement offered by fibres was not effective to significantly increase the post-peak behaviour. Hence, the increment in toughness was not significant compared to higher dosages. The failure modes of cylinders due to the addition of fibres are shown in **Figure 3**. The peak compressive strength of the cylinder is in the range of 52 MPa - 54 MPa.

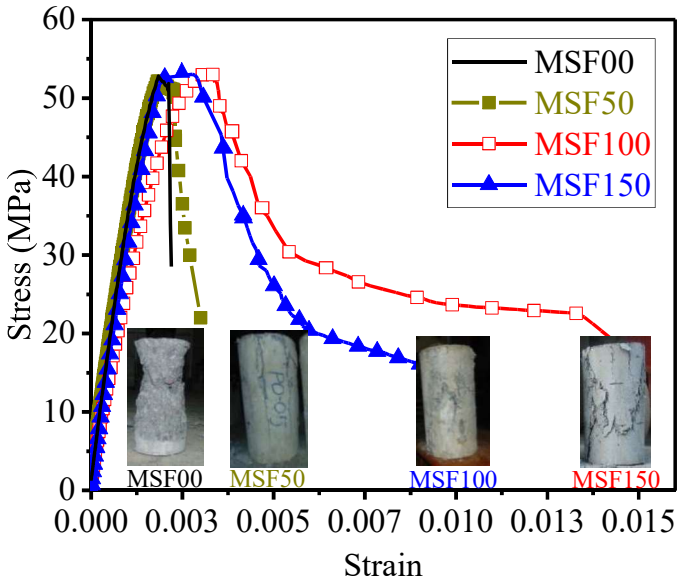

Figure 3. Stress-strain curve of concrete cylinders in compression

Table 3. Properties of MSFRC in Compression

Mix ID	Cube strength (MPa)	SD (MPa)	Cylinder strength (MPa)	SD (MPa)	Toughness (A_f)	Toughness index (T.I $=A_f/A_c$)
MSF00	57.91	1.46	52.75	1.05	0.0738	1.00
MSF50	59.23	1.30	53.46	1.26	0.1028	1.40
MSF100	67.08	1.27	53.62	0.83	0.2805	3.80
MSF150	68.12	1.18	54.14	1.10	0.4239	5.74

Note: SD = Standard deviation (MPa), A_f = area of the stress-strain curve of the fibre-reinforced concrete cylinder, A_c = area of the stress-strain curve of the control cylinder

The tension stiffening response of fibre reinforced concrete depends on the characteristics of fiber such as aspect ratio, length, types, the volume fraction of fibers, as well as matrix properties such as strength and aggregate size. Few researchers [34–39] in the past have studied the influence of fibre orientation factor on the mechanical performance of FRC, such as strength, load-CMOD, and fracture energy. They noted a considerable improvement in post-peak response due to the orientation effect [34,37,40]. The increment in post-peak response leads to an increase in residual flexural tensile strength (f_R). Thus, the ductility of fibre-reinforced prestressed concrete beams can

be increased in both flexure and shear dominant loading. However, the effect of fibre orientation is not considered in this study and is scope for further work.

3.2 Fracture Tests

Concrete prisms were cast and tested under a three-point bending test as per EN14651 (2005). The size of the prism is 150 mm x 150 mm x 500 mm. A notch of 25 mm depth and 5 mm width was prepared in the prism to localize the damage in a defined position. The crack width is monitored by crack mouth opening displacement (CMOD) and crack tip opening displacement (CTOD) gauges. Similarly, one LVDT is used to monitor the vertical deflection of the prism. A non-contact digital image correlation (DIC) technique was used to monitor full-field strain measurements and to study crack propagation. The DIC system consists of two light sources, one high-resolution camera, and a storage device, as shown in **Figure 4 (a)**. In the pre-processing phase, the notched beams were painted and speckled with black colour ink with a speckling gun [41]. After mounting all the gauges, the calibration image is captured before the start of testing. After that, images were captured at specific intervals according to the rate of loading. All the FRC prisms were tested under displacement control mode with a 5mm/min rate by using a flexure testing machine, as shown in **Figure 4 (a)**.

The load-CMOD response of MSF00, MSF50, MSF100, and MSF150 concrete prisms are presented in **Figure 4 (b)**. The response shows that the post cracking behaviour was significantly improved due to the addition of 0.5%, 1.0%, and 1.5% of volume fractions of MSF compared to control (MSF00) beams. In control prisms (MSF00), the obtained peak load is 14 kN, which is the same as that of the MSF100 prism. However, MSF100 prisms also had a second peak load of 9.31

kN, which occurred at CMOD of 2.3 mm. Thus, macro synthetic fibre addition did not change the first cracking load but significantly improved the post cracking behaviour. Similarly, in MSF50 beams, the second peak load of 4kN is observed at a CMOD of 2.5 mm. Hence, from this experimental response, it is concluded that the MSF fibres of aspect ratio 100 can effectively engage in strain redistribution at higher crack openings such as 2.5 mm of CMOD. The load-CMOD curves were used to obtain the tensile stress-strain response from the inverse analysis. The multi-linear tensile stress-strain behaviour of specimens with different fibre volume fractions was obtained from the inverse analysis. More information on inverse analysis can be found elsewhere [42].

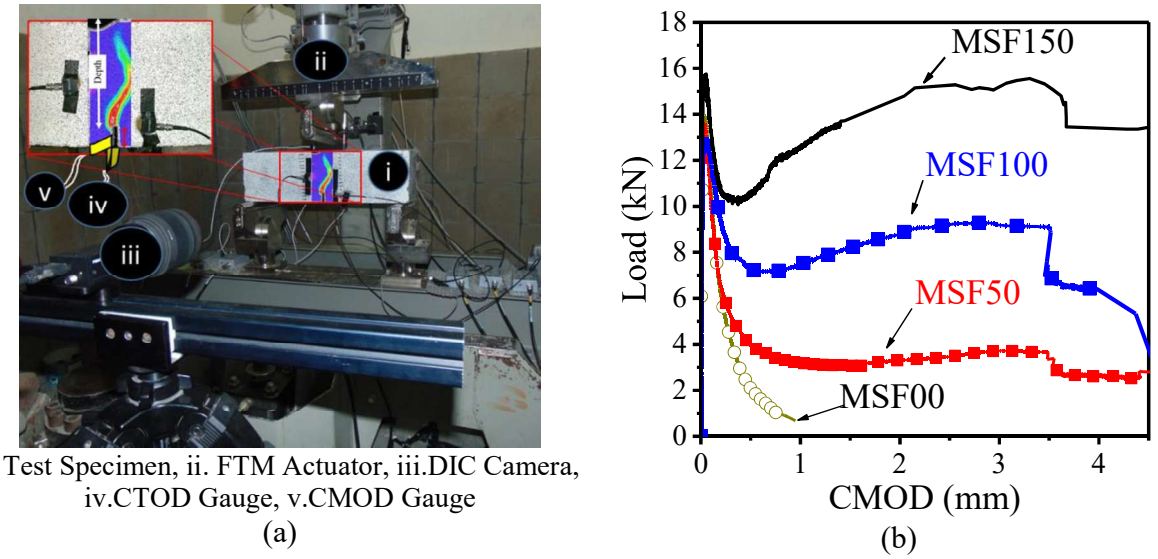

i. Test Specimen, ii. FTM Actuator, iii.DIC Camera, iv.CTOD Gauge, v.CMOD Gauge

(a) (b)

Figure 4. Fracture tests on MSFRC Prisms (a) Test setup, (b) Load-CMOD curve

The average residual flexural tensile strength (f_{R1} to f_{R4}) of MSFRC prisms was calculated based on RILEM recommendation[43]. Here, f_{R1}, f_{R2}, f_{R3}, and f_{R4} are calculated at CMOD of 0.5mm, 1.5mm, 2.5mm, and 3.5mm respectively. The fracture energy (G_f) of prisms was calculated based on the provisions of the Japan concrete institute (JCI) code [44]. The improvement in fracture energy due to the addition of 0.5%, 1.0%, and 1.5% volume fraction of MSF fibres are 4.55, 9.62,

and 16.03 times that of the control prism (MSF00). The residual flexural tensile strength of MSF prism was calculated based on the RILEM [43] recommendations and presented in **Table 4**. The DIC strain contours were used (**Figure 5**) for understanding the crack initiation and crack propagation at different CMOD values[21].

Table 4. The residual flexural tensile strength and fracture energy of prisms

Mix ID	Residual flexural tensile strength (MPa)				Total fracture energy (N-mm)	The ratio of Fracture Energy (ΔG_f)
	f_{R1}	f_{R2}	f_{R3}	f_{R4}	G_f ($\times 10^{-3}$)	$\Delta G_f = \frac{G_f}{G_{fc}}$
MSF00	0.69	-	-	-	156.7	1.00
MSF50	1.14	0.88	1.00	0.97	713.2	4.55
MSF100	2.10	2.36	2.65	2.62	1506.7	9.62
MSF150	3.04	4.00	4.39	4.34	2512.5	16.03

In control prisms (MSF00), the crack propagated without the formation of any strain localization, as shown in **Figure 5 (a)**. However, in the case of MSF50 beams, the strain localization started at a CMOD of 1.5 mm. Similarly, in MSF100 beams, the number of hinge formations was more along the cracked surface compared to MSF50 beams. The crack initiated and propagated in MSF beams from the tension zone to the loading point progressively, and the propagation of the tip of the crack can be visualized in **Figure 5**. The strain contours from DIC analysis help understand the reason for a significant increase in the second peak in loading **Figure 4 (b)-(d)**. The hinges formed along the depth of the beam due to the bridging action of fibres against the crack opening, as shown in **Figure 5**. The detailed discussion about the formation of hinge and comparison with different fiber dosages were discussed in the previous work of authors [21].

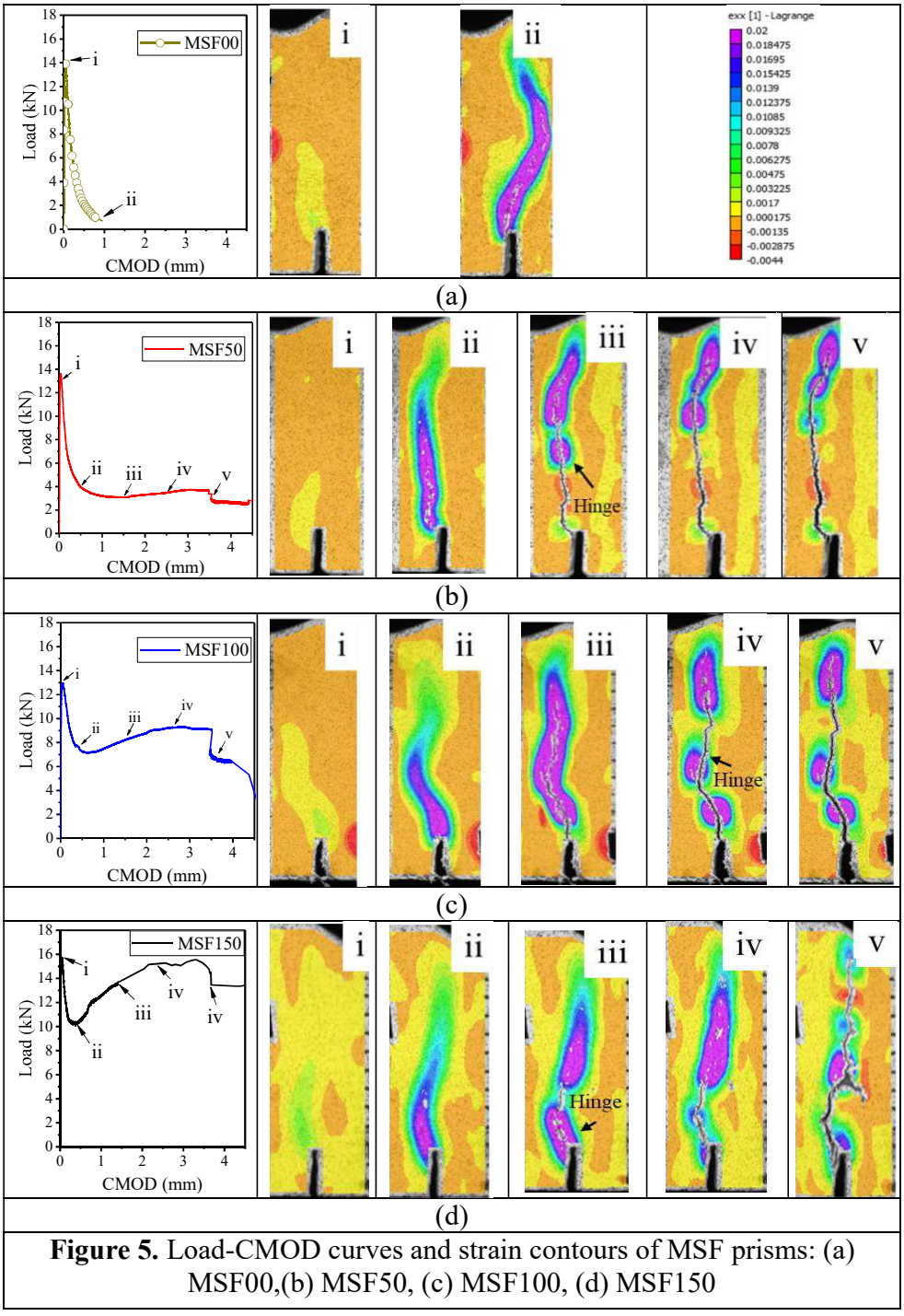

Figure 5. Load-CMOD curves and strain contours of MSF prisms: (a) MSF00,(b) MSF50, (c) MSF100, (d) MSF150

3.3 Stress-Strain Curve of Prestressing Strand

The seven-wire low relaxation prestressing strand of 12.7 mm diameter was tested under tension to get the stress-strain response. An extensometer and strain gauges were mounted to measure the

strains, as shown in **Figure 6 (b)**. The test is performed according to ASTM A1061 [45] with the help of a servo-controlled fatigue testing machine (FTM) as shown in **Figure 6**. The obtained stress-strain response of prestressing strand is shown in **Figure 6 (c)**. The average tensile strength of the prestressing strand is 1860 MP with an elastic modulus of 196 GPa (**Table 5**). The same test results were used for nonlinear finite element analysis simulation after converting the engineering stress-strain curve to the true stress-strain curve.

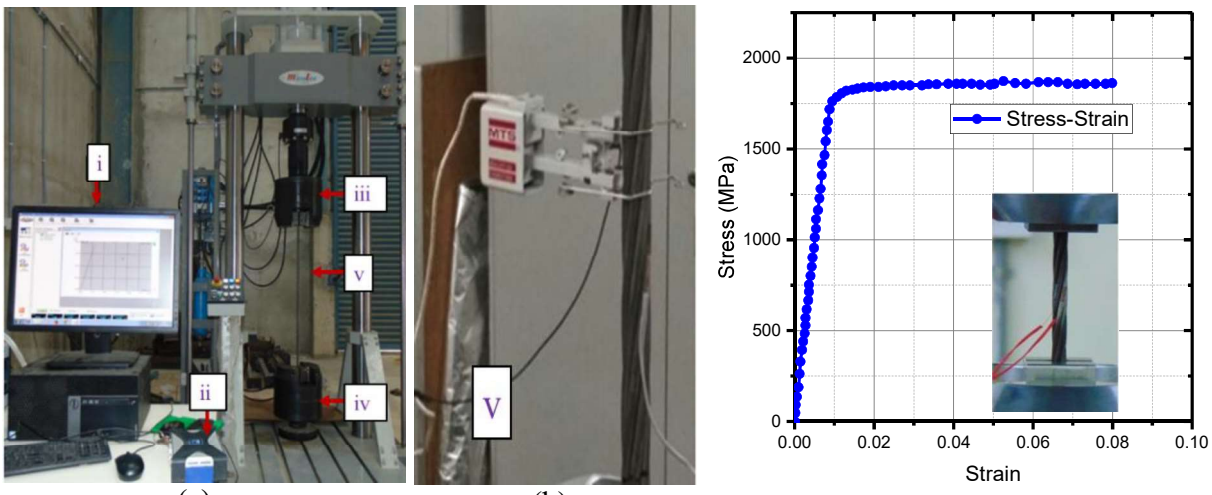

(a) (b) (c)

i-monitor, ii=Data acquisition system, iii=Upperlimb, iv-Lowelimb, v=Prestressing strand with clip-gauge

Figure 6. Coupon test of HTS strand: (a) Fatigue testing machine, (b) Extensometer, (c) Prestressing strand stress-strain curve

Table 5. Mechanical properties of prestressing strand

Avg. Tensile strength (MPa)	f_{yp}	1860
Area of cross-section (mm^2)	A_p	98.4
Modulus of elasticity (MPa)	E_p	196500
Poisson's ratio	γ	0.3

3.4 Testing of Prestressed Concrete Beams

The prestressed concrete beams of size 150 mm × 300 mm × 1600 mm were cast with MSFRC concrete (0.0%, 0.5%, 1.0% and 1.5% V_f of macro-synthetic fibers). In total, eight prestressed concrete beams were tested under shear-dominated loading, as shown in **Figure 7**.

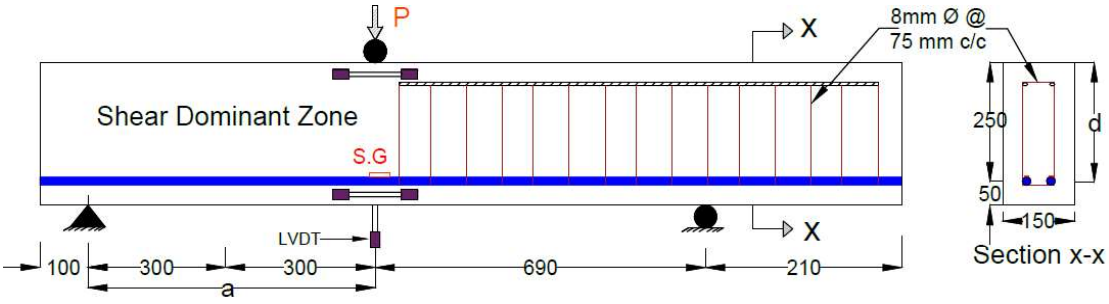

(a)

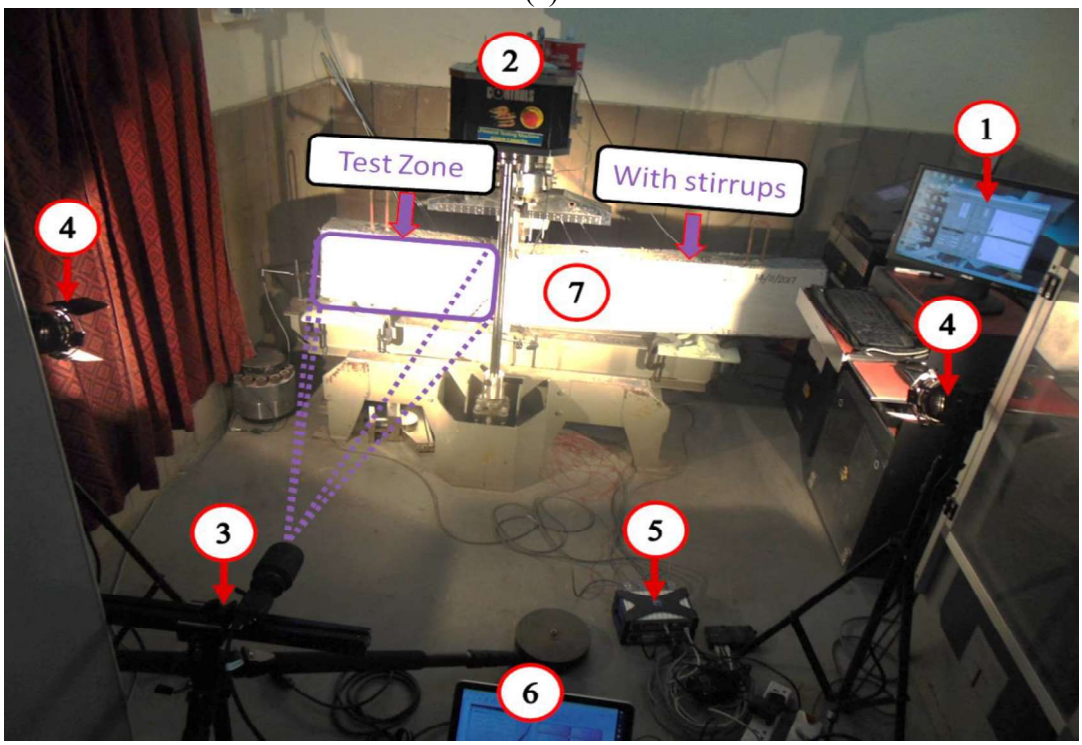

1. Controller, 2. Test frame of 300KN capacity, 3.DIC camera, 4. The light source, 5. Data Acquisition system (DAC), 6. DAC data storage (DAC+DIC) and 7. Specimen

(b)

Figure 7. Prestressed concrete beam details along with (a) Instrumentation, (b) Test setup

Two LVDTs were used at the loading point for monitoring the deflection of beams. The strain in strands is monitored using strain gauges bonded on the prestressing strand. The level of prestressing applied in these beams is 40% to that of the ultimate capacity of the prestressing strand (1860 MPa). A prestressing force of 154.5 kN was applied at an eccentricity of 100mm. Due to this, average compressive stress of 3.43 MPa is produced. A DIC setup was used for tracking the crack initiation and propagation and for strain measurements in the test zone. The images of deformed specimens are captured at the same rate of loading in the shear dominant zone of the specimen. After that, post-processing is carried out by using VIC-2D^{TM} package. All the prestressed concrete beams were tested using displacement control mode at a rate of 0.025mm/sec. In each series, two prestressed concrete beams were tested to ensure the consistency of test results.

4.0 TEST RESULTS AND DISCUSSION

4.1 Control beam (MSF00)

The complete load-deflection response of macro synthetic fibre-reinforced prestressed concrete (MSFRPC) beams are shown in **Figure 8**. The first shear crack in MSF00 was initiated at a load of 178 kN and deflection of 2.9 mm (**Figure 9)**. By strain contours from DIC measurements, the crack initiation and propagation path can be identified. MSF00 reached a peak load of 216.3 kN at a deflection of 4 mm. After reaching the peak load, a shear crack formed at an angle of 41.2° due to diagonal shear tension. The energy absorption capacity is calculated as the area under the load-deflection curve up to the ultimate load point. The ultimate load (P_u) point is considered as a 20% drop from the peak load (P) [18]. The average energy absorption capacity of the control beam is measured as 785.8 (kN-mm), and the failure mode is observed as direct shear tension (*DST*).

4.2 MSFRPC beams (MSF50)

The load-deformation behaviour of the MS50 beam with a volume fraction of 0.5% is shown in **Figure 8**. The peak load of MSF50 was 264.6 kN at the deflection of 4.8 mm. The peak load increased by 21.4% when compared with a control beam (MSF00). The first shear crack initiated in MSF50 beams at a load of 160.6 kN at a deflection of 2.1 mm (**Figure 9)**. MSF50 reached a peak load of 264.6 kN at a deflection of 4.8 mm, and shear crack is formed at an angle of 45.8°. The average energy absorption capacity of the MSF50 beam is obtained as 2918.2 kN-mm, which is 3.72 times more than that of control beams. A low fibre dosage of 0.5% could not change the failure mode, and MSF50 failed in direct shear tension failure mode.

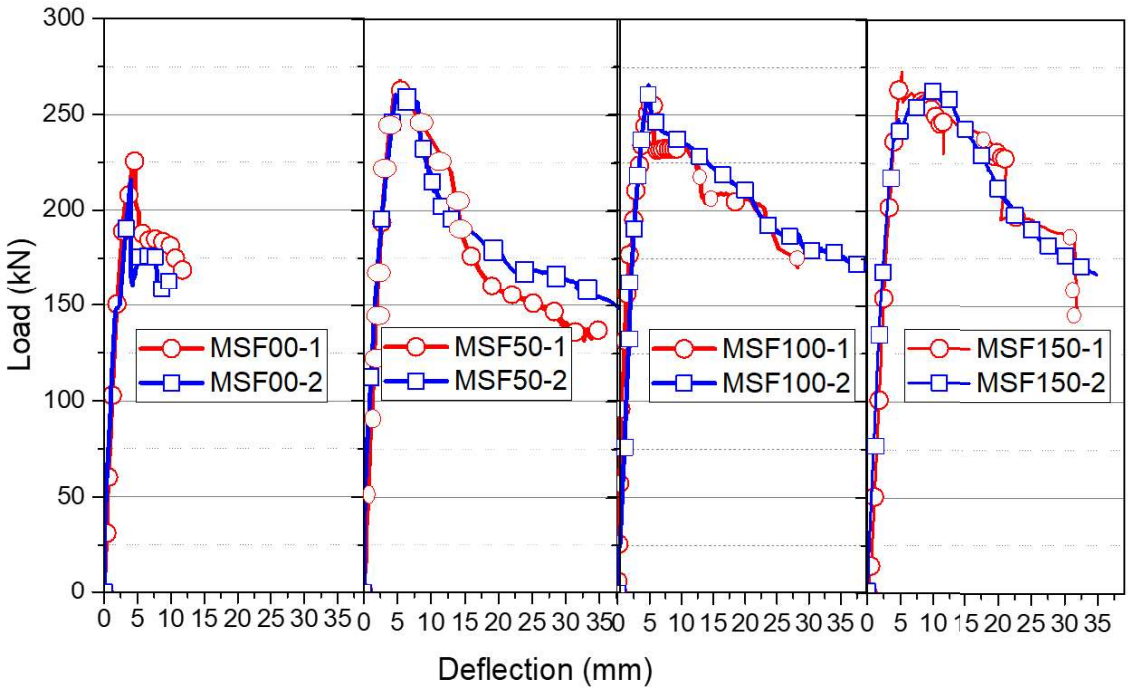

Figure 8. Load-deflection response of PO00, PO50, PO100, and PO150 beams

4.3 MSFRPC beams (MSF100)

The shear crack in MSF100 was initiated at a distance of 375.3 mm from the support (**Figure 9)**. The same crack propagated towards the loading point with an angle of 47°. The improvement in

peak load is 40 kN to that of control beams (216 kN). This increase in peak capacity is due to the fibre bridging action, which restrained the crack opening. Similarly, the improvement in ultimate load is about 21.2% to that of the control beam. The strain contour plots of MSF100 beams (**Figure 9**) showed more distributed cracks occurred at peak and ultimate load due to the presence of fibres. Also, the failure angle did not change much even with the addition of high fibre dosage. However, MSF100 beams failed in the ductile mode, as shown in **Figure 9**.

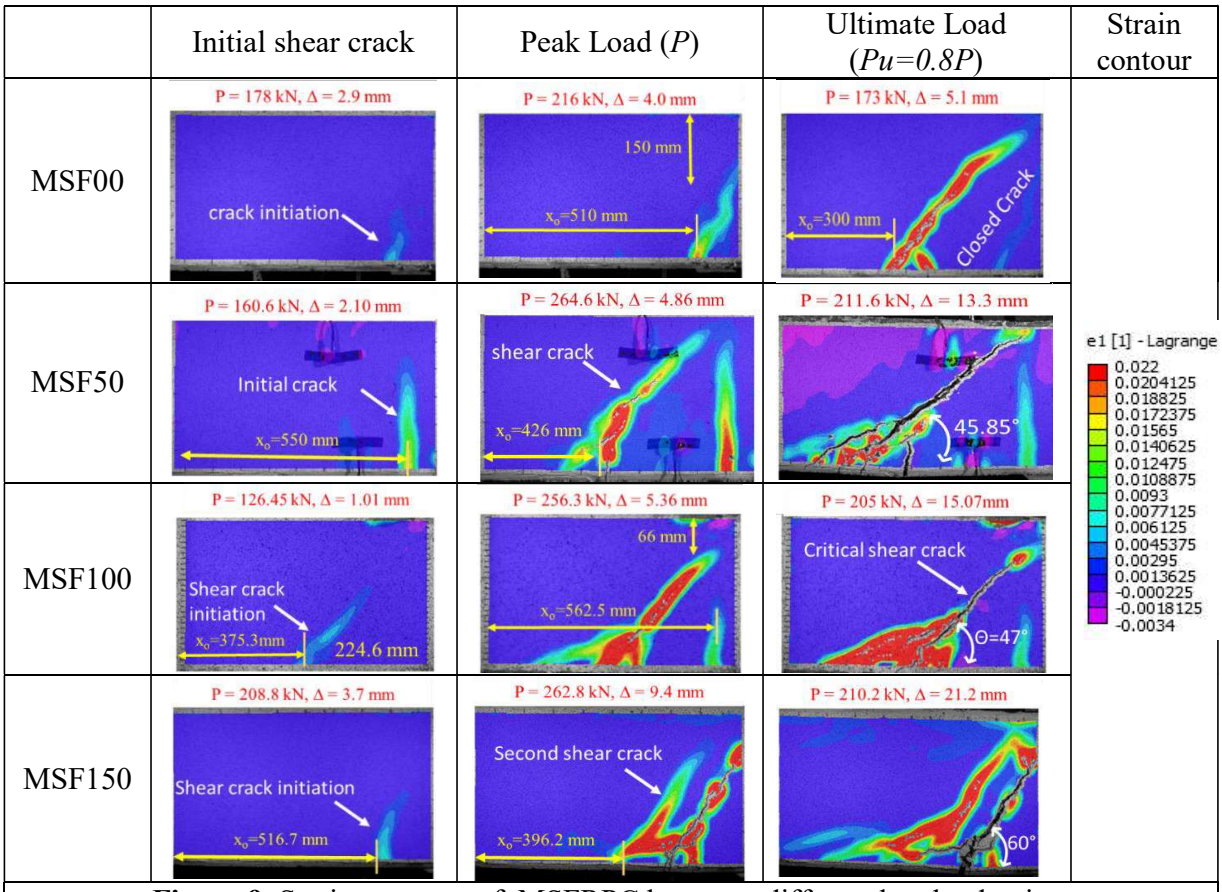

Figure 9. Strain contours of MSFRPC beams at different key load points

Energy absorption capacity (EAC) also increased significantly due to fibre addition (**Table 6**). The improvement is EAC due to the addition of 1.0% of macro synthetic fibres is 4.0 times that of control beams. A significant increase in EAC indicates the addition of fibres helps in absorbing the sudden energy release (control beams) and thereby converts the brittle failure to ductile mode.

4.4 MSFRPC beams (MSF150)

The MSFRPC beams reinforced with a 1.5% volume fraction of macro synthetic fibres reached a peak load of 272.7 kN. Also, the improvement in EAC is 6.0 times that of control beams. The fibres contributed effectively to strain redistribution, due to which the post-peak response increased reasonably. Similarly, the ultimate load improvement is about 26% to that of the control beam is observed. From the strain distribution plots of MSF150 beams, it is observed that more distributed cracks occurred along with new shear cracks at peak and ultimate load. Moreover, due to the higher dosage of fibre addition, the crack angle of the critical crack increased from 41° to 65°. MS150 beams failed in ductile mode, as shown in **Figure 9**. From experimental results, it is observed that the beam reached its ultimate load at the deflection of 21 mm (**Table 6**).

Table 6. Summary of test results of MSFRPC Beams

Beam ID		A	B	C	D (kN-mm)	θ (°)	Failure mode
MSF00-1	Load (kN)	178	216.3	173.0	785.8	41.2	DST
	Δ (mm)	2.9	4.0	5.1			
MSF00-2	Load (kN)	167	224.5	179.6	741.5	42.4	DST
	Δ (mm)	2.6	4.2	5.3			
MSF50-1	Load (kN)	160.6	262.6	211.6	2918.2	45.8	DST
	Δ (mm)	2.1	4.8	13.3			
MSF50-2	Load (kN)	158.8	260.2	208.2	2298.8	45.0	DST
	Δ (mm)	2.6	4.7	10.9			
MSF100-1	Load (kN)	126.5	256.3	205.0	3183.5	47.5	DST
	Δ (mm)	1.0	5.3	15.0			
MSF100-2	Load (kN)	131.2	262.2	209.7	3184.8	49.3	DST
	Δ (mm)	1.2	5.4	15.2			
MSF150-1	Load (kN)	159.2	272.7	218.2	4742.8	65.3	FS
	Δ (mm)	2.5	5.3	21.4			
MSF150-2	Load (kN)	208.8	262.8	210.2	4733.7	60.2	FS
	Δ (mm)	3.7	9.4	21.2			

Note: A = Shear crack load (kN), B = Peak load (kN), C = Ultimate load (kN), D = Energy absorption capacity (EAC) (kN-mm), θ = Failure crack angle, DST= Direct shear tension, FS=Flexure shear.

4.5 Discussion

The control prestressed concrete beams cracked at a distance of 510 mm from support. After peak load, the new crack is initiated at a distance of 300 mm from support, as shown in **Figure 9,** and the beam collapsed in brittle mode. However, MSF50 beams with 0.5% volume fraction, a flexural crack initiated at a distance of 550 mm from support. At peak load point, it cracked in shear at a distance of 426 mm from support and led to final failure under direct shear tension mode. Similarly, the MSF100 beams with 1.0% of fibre volume fraction had a shear crack at a distance of 375.3 mm from support but did not fail in a brittle manner. The MSF150 beams had a flexure-shear crack at a distance of 516.7 mm. With the increase in applied loads, the same crack propagated towards the loading point at an angle of 60°. Other than MSF100 beams, the critical crack initiation length increased with an increase in fibre volume fraction. Similarly, the crack propagation rate reduced with an increase in the dosage of fibres.

After the failure of specimens, the fibre distribution in a cracked plane is measured to understand the nature of fibre distribution. The failure plane of prestressed fibre reinforced concrete beams was divided into several grids, as shown in **Figure 10** with an offset of 50 mm in both horizontal and vertical directions. The fibre distribution in MSF50 was 65 to 75 numbers in a 50 mm grid. Similarly, in both MSF100 and MSF150 beams, the number of fibres across the cracked plane increased significantly, as shown in **Figure 10 (b)**. Fibre distribution was found to be even across the depth of the failure plane. Both the rupture and pull-out failure of fibres were observed.

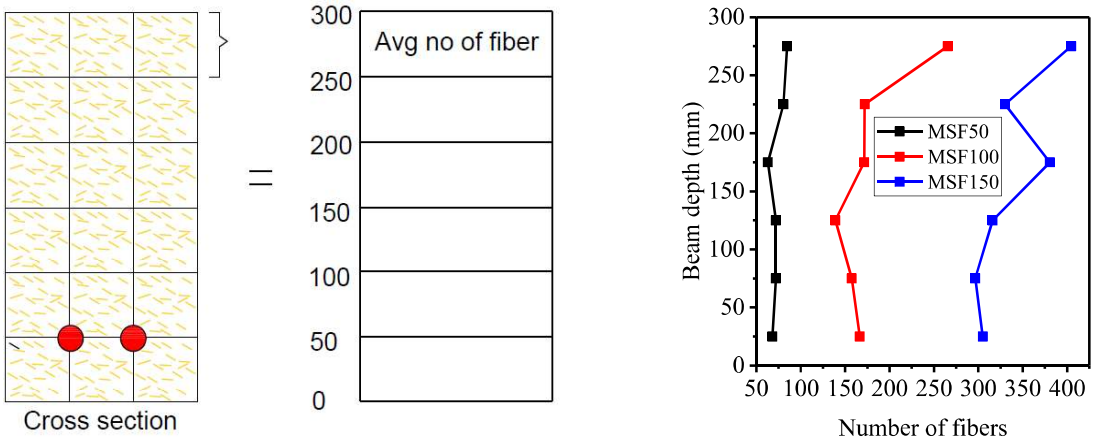

Figure 10. Fibre distribution across the depth of MSFRPC beam: (a) Grid with 50 mm x 50 mm spacing, (b) Average number of fibres across the depth

5.0 FINITE ELEMENT STUDIES

Three-dimensional FE models of test beams were created using finite element software ABAQUS. Concrete is modelled using C3D8R element with concrete damage plasticity model (CDP) as a material model. The prestressing strand and steel reinforcement were modelled using the truss element (T3D2). The stage-wise analysis is performed for prestressing and the applied shear loading.

5.1 Material Properties

Test specimens had an average compressive strength of 54 MPa, and the same is used for FE model. The stress-strain response of high-strength concrete without fibres in compression is modelled using the Thorenfeldt model[46]. Similarly, the stress-strain response of fibre reinforced concrete under compression is modelled using Yu-Chen et al. [47] model. The tension-stress strain behaviour is obtained from the inverse analysis developed by Bhosale et al. [42]. The stress-inelastic strain in both compression and tension for FRCs with different fibre dosages are shown in **Figure 11**.

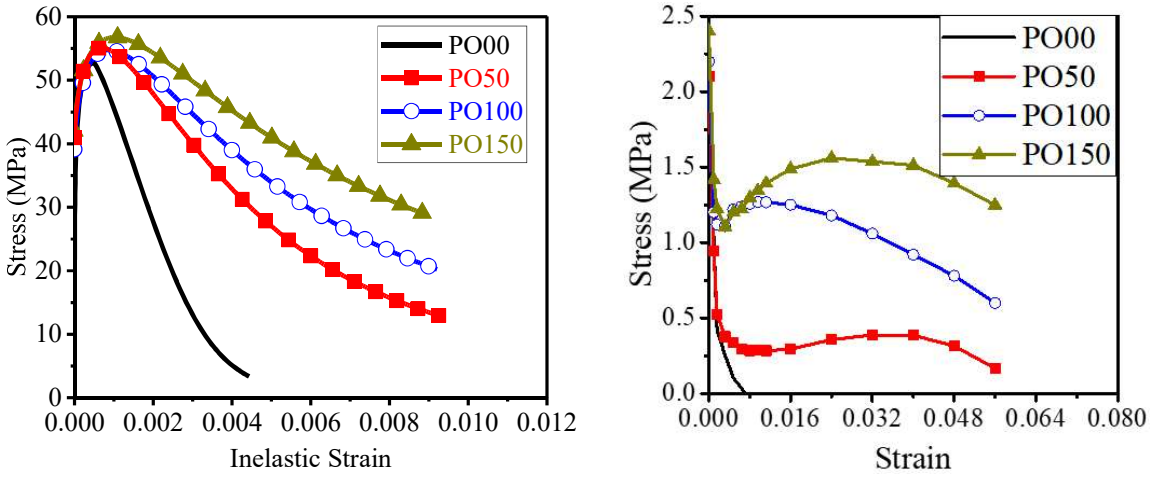

Figure 11. MSF concrete stress-strain properties: (a) Compression, (b) Tension

The damage in compression (d_c) and damage tension (d_t) is calculated as per **Equation (1) - Equation (2)** based on Huang and Liew [48]. The damage variables are a function of stress, elastic modulus, and strain in concrete.

$$d_c = 1 - \frac{\sigma_c + n_c f_{ck}}{E_c(n_c\sigma_c / E_c + \varepsilon_c)} \quad (1)$$

$$d_t = 1 - \frac{\sigma_t + n_t f_t}{E_c(n_t\sigma_{to} / E_c + \varepsilon_t)} \quad (2)$$

Where σ_c is stress, and f_{ck} is the compressive strength of concrete, E_c is the elastic modulus of concrete, n_c and n_t are the constant factors for compression and tension respectively, ε_c is the concrete strain in compression, and ε_t is concrete strain in tension which should be larger than zero. The notched beams reinforced with macro synthetic fibre were tested. The fracture energy (G_f) is calculated as per JCI-S-001-2003[49]. The tensile strength from the inverse analysis [42] is used as tensile behaviour as input for concrete. The multi-linear stress-strain response obtained from inverse analysis (**Figure 11**) is used as input for inelastic strain and damage (d_t) parameters.

5.2 Concrete Damage Plasticity Model (CDPM)

The concrete damage plasticity model (CDPM) is widely used to represent the complex behaviour of quasi-brittle material like concrete. This model is used for modelling concrete under both monotonic and cyclic loading [27]. A three-dimensional eight-node element (C3D8R) in ABAQUS is used for modelling concrete. The stress-strain response of concrete includes elastic and plastic properties. The total strain of concrete is the combination of both elastic and plastic strains. The nonlinear portion of the stress-strain response of concrete represents the plasticity and damage response. Hence, it is essential to define the damage corresponding to the plastic strain of concrete. The damage variables in concrete represented as d_c and d_t compression and tension damage, respectively. The damage is identified in the range of 0 to 1. Here, 0 represents no-damage, and 1 represents full damage [7,26,50–52]. The yield criteria define the critical stress state beyond which plastic deformation initiates and leads to failure. Many researchers have developed a yield criterion based on strength under compression and tension [27,28]. A similar approach is adopted as CDPM in ABAQUS. Few researchers performed the test on concrete in different conditions such as uniaxial tension, biaxial tension, uniaxial compression and biaxial compression and developed failure envelopes [26,51]. For brevity, details on CDPM are not provided here and can be found elsewhere (ABAQUS [53]).

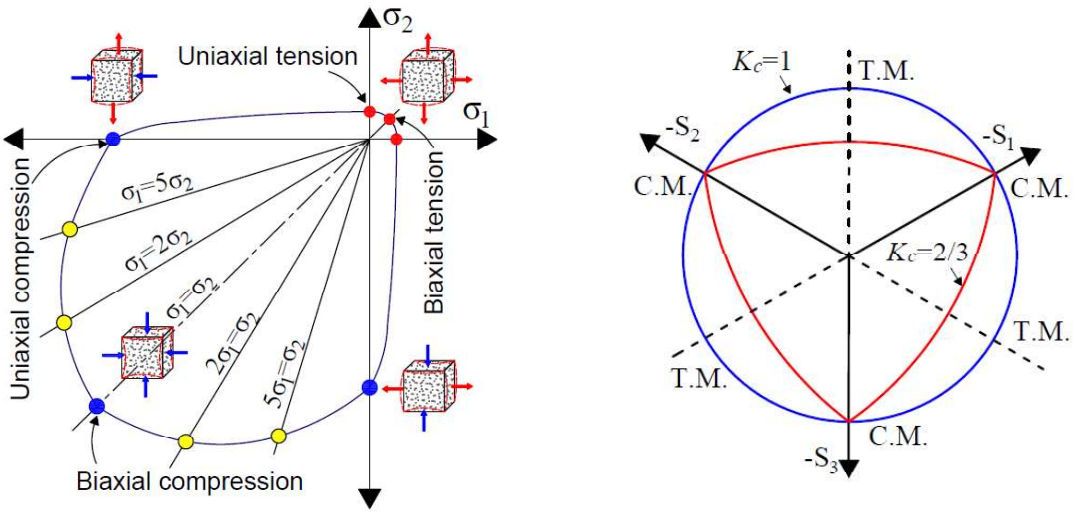

(a) (b)

Figure 12. Yield criteria of concrete: (a) Concrete strength under biaxial stress, (b) Deviatoric cross-sections of the failure surface

350

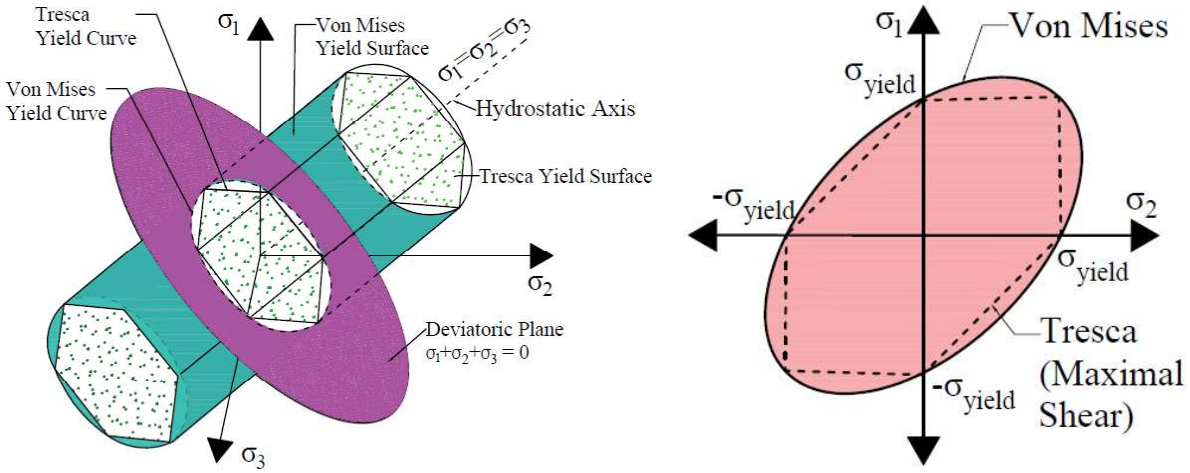

(a) (b)

Figure 13. The different failure criterion for different stress models: (a) 3D schematic view, (b) Yield surface in 2D

351

352 The plasticity constants of concrete include dilation angle, eccentricity, stress ratio, shape factor,

353 and viscosity parameter are shown in **Table 7**. The schematic view of yield criteria concrete and

354 failure criteria are shown in **Figure 12** and **Figure 13**. Previous research shows that the dilation

355 angle plays an important role in predicting peak load, post cracking behaviour, and failure mode

of beams [54–59]. From the sensitivity analysis, the dilation angle is chosen as 52.3˚ to simulate the experimental results closely. Other plasticity parameter values such as eccentricity, stress ratio, and shape factors are selected, such as default values. The analysis was carried out using ABAQUS/Standard, and the viscosity parameter term is activated [56]. The viscosity parameter is taken as 0.0005 for better convergence of the solution.

Table 7. Plasticity constants of concrete

Dilation angle (φ)	Eccentricity (ϵ)	F_{bo}/F_{co}	K_c	Viscosity Parameter (μ)
53.2°	0.1	1.16	0.667	0.0005

5.3 Prestressing Strands and Stirrups

The prestressing strand of length 1600 mm and with a cross-section of 98.4 mm^2 is modelled as a linear truss element (T3D2). The stress-strain properties of the strand were measured by a direct tension test, as shown in **Figure 6**, as explained in the experimental program. The same properties were converted as true stress-strain curve and implemented in FEM simulation. The pre-tensioning can be simulated by various modelling techniques such as initial stressing (default method). An initial prestress of 782.9 MPa is applied in each strand. The steel reinforcement of diameter 8 mm is used as secondary reinforcement. These secondary reinforcements were assigned with linear truss element (T3D2). The location of the stirrups and top reinforcement details are shown in **Figure 14 (a)**. Steel reinforcement is assumed to have elastic modulus (E_{st} = 2 x 10^5 MPa) and Poisson's ratio of 0.3. Both the high-strength prestressing strand and rebars were embedded in concrete. The embedment technique enables one or more elements to be embedded inside the host element. This technique does not require the modelling of the contact surface, and it eliminates the calculations of surface formulations [60]. The rebar node is defined as a master node, and

surrounding concrete is assigned as slave nodes, as shown in **Figure 14 (b)**. The rebar nodes lie in the concrete element. Hence, the translation degrees of freedom of steel rebars is tied with that of the concrete element.

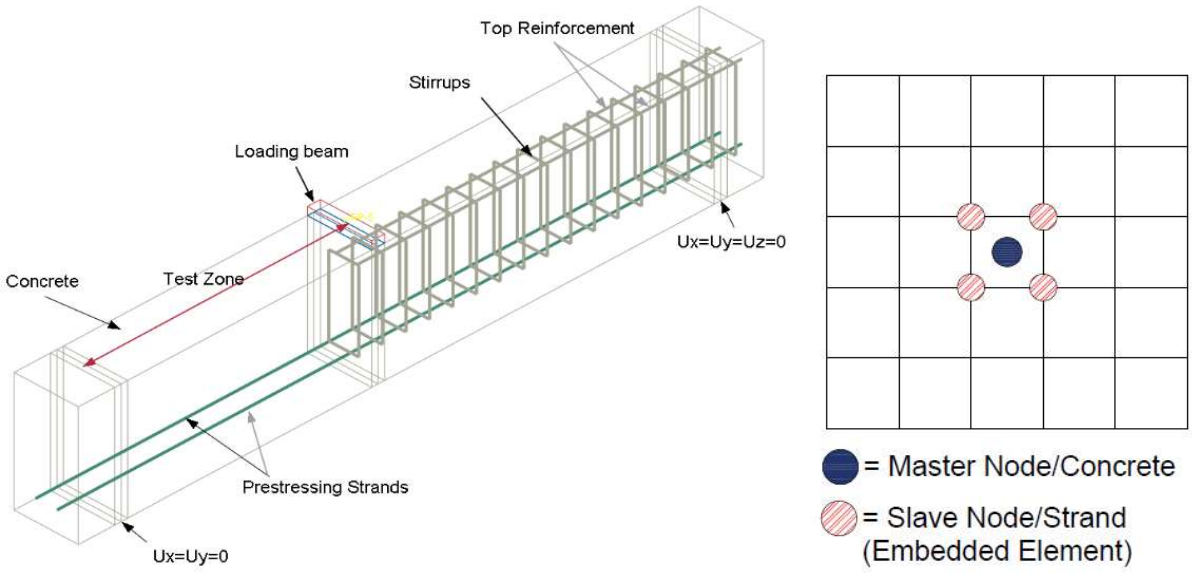

(a) (b)

Figure 14. FE Modelling (a) Schematic view of prestressed concrete beam elements, (b) Strand slave nodes and concrete master nodes

5.4 Loading and Boundary Conditions

Loads were applied in two stages. The prestressing load was applied in the first stage, followed by the external load in a displacement control mode. Simple support boundary conditions are imposed in FEM modelling, as shown in **Figure 14 (a)**.

5.5 Load-Deflection Behaviour and Failure Modes

FE models of fibre-reinforced prestressed concrete beams with different dosages were developed and analysed. The load-deflection behaviour and failure modes are shown in **Figure 15** and **Figure 16**, respectively. The load-deflection response of control (MSF00) and fibre reinforced concrete

beam (MSF50 and MSF100) is predicted well up to the ultimate load. In the case of MSF150 beam, the load-deflection behaviour is little offset to that of observed behaviour. The failure mode of all the prestressed concrete beams was in direct shear tension. The comparison between experimental and FE simulation responses are shown in **Figure 16**.

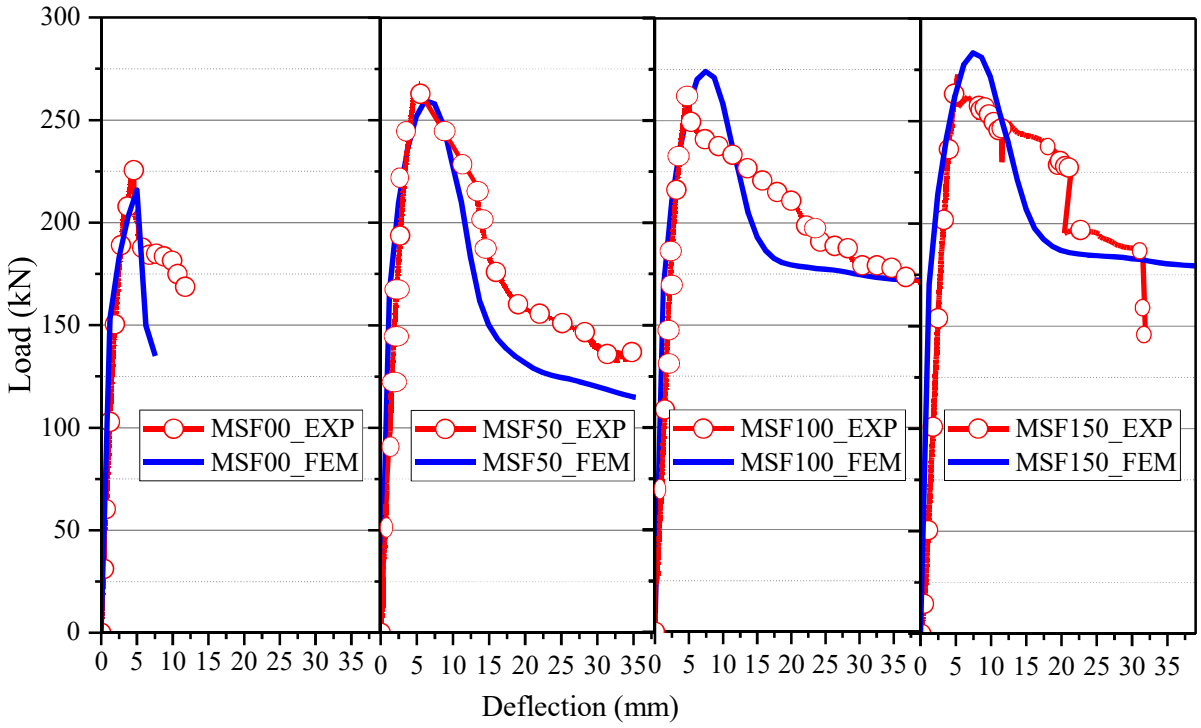

Figure 15. Load-deflection response of MSFRPC beams subjected to shear dominated loads

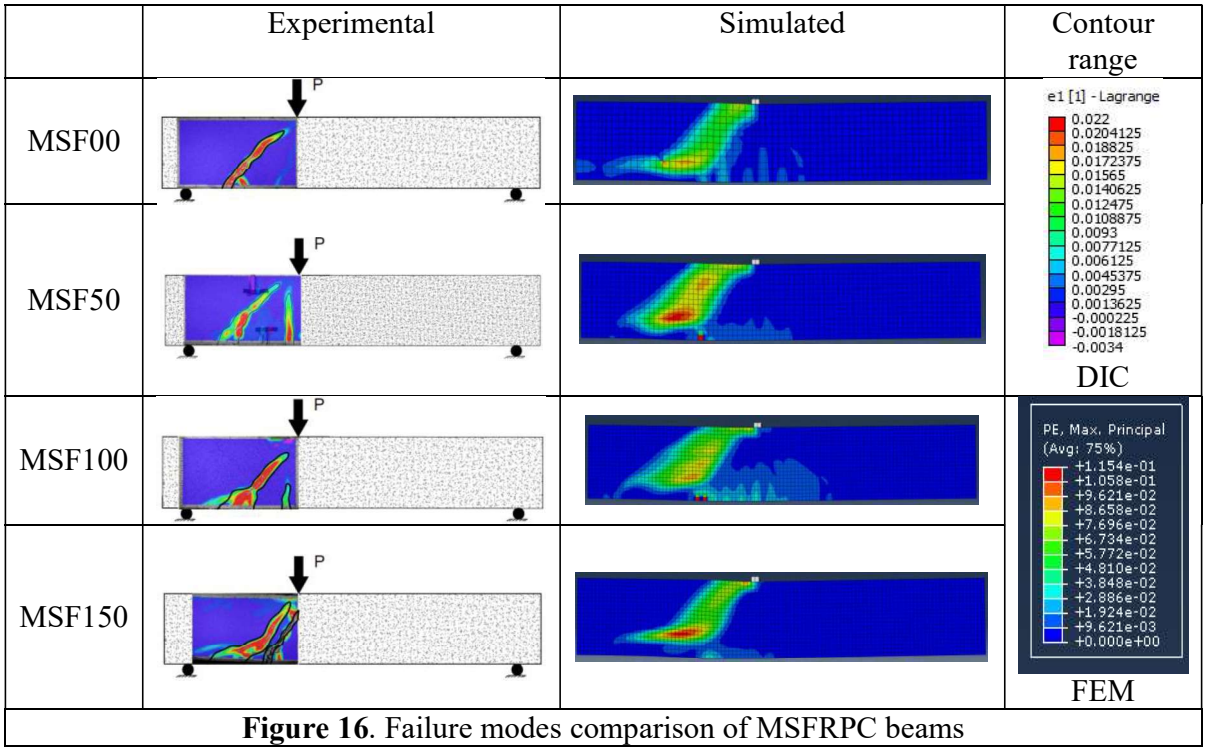

Figure 16. Failure modes comparison of MSFRPC beams

5.6 Parametric Studies

The shear capacity of prestressed fibre reinforced concrete beams depends on the concrete compressive strength, level of prestressing, shear reinforcement ratio, and fibre volume fraction. Experimental validation of 0.0%, 0.5%, 1.0% and 1.5% volume fraction were studied. In this parametric study, the influence of the prestressing level is focused on the different volume fractions of fibres at the same shear span to depth ratio of 2.4. With the increase in the level of prestressing, the shear capacity of the beams increased, as shown in **Figure 17**.

The increase in the prestress level does not increase the shear strength significantly for the control beam (MSF00). For a higher prestress level of 0.8 P_u, the specimen failed in a premature shear compression mode. In fibre-reinforced beams, a limited increase in shear strength (between 9% to 11%) was observed due to an increase in prestress levels. **Figure 17** shows that there is not much

improvement in shear capacity after 60% of increment in prestressing. The MSFRPC beams of different levels of prestressing, such as 60%, 70%, and 80% failed in shear mode, as shown in **Figure 18**. The shear strength is enhancement is due to prestressing, which delayed the formation of shear cracks and helped in controlling the crack opening.

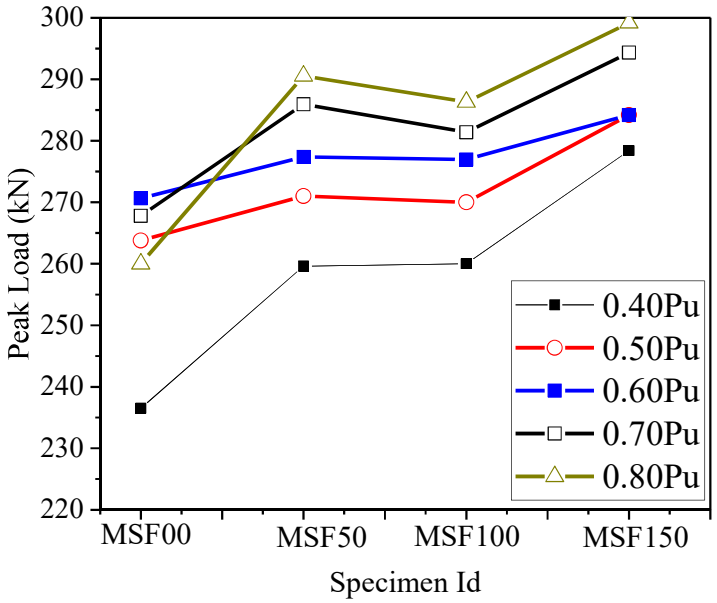

Figure 17. Parametric study on the level of prestressing

Beam ID	$0.6P_u$	$0.7P_u$	$0.8P_u$
MSF00	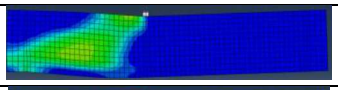	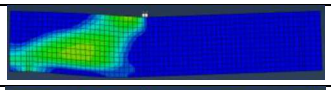	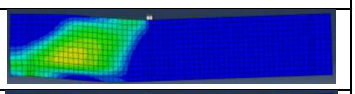
MSF50	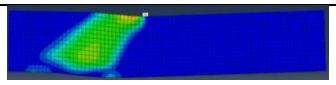	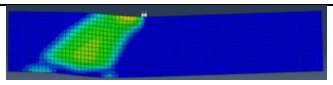	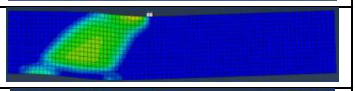
MSF100	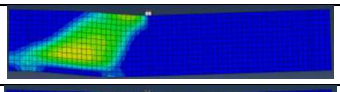	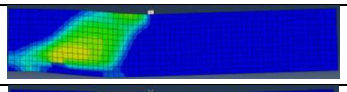	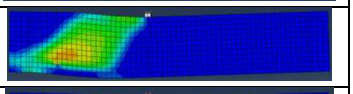
MSF150	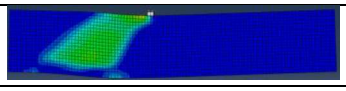	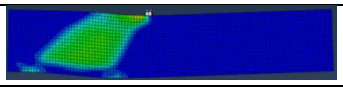	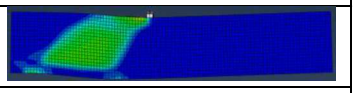

Figure 18. Failure modes of MSFRPC beams at different level of prestressing

6.0 SHEAR CAPACITY PREDICTIONS BY RILEM AND FIB-MC2010 PROVISIONS

The shear capacity of MSFRPC beam is calculated by using RILEM [43] and Fib- MC2010 [61] code provisions. The average tensile strength of FRC as per RILEM provisions is used for estimating the shear capacity of beams.

6.1 Shear capacity calculations using RILEM recommendations (V_{RILEM})

The shear capacities (V_{RILEM}) formulations in RILEM recommendations [43] include three components such as shear resistance of member without shear reinforcement (V_{cd}), shear resistance due to discrete fibres (V_{fd}) and shear reinforcement/stirrup contribution (V_{wd}). The shear resistance of member without shear reinforcement (V_{cd}) includes the resistance due to un-cracked concrete, aggregate interlock, dowel action, and initial prestress. Similarly, shear resistance due to fibres (V_{fd}) includes factor accounting for the flange of T-sections and depth factor. The flange contribution is taken as one for rectangular beams. Other parameters were calculated as per the sectional details of the test specimens. The resistance offered by fibres in tension at a CMOD of 3.5 mm is used for shear contribution of fibres. These residual flexural tensile strengths vary based on fibre dosage and type of fibres and strength of concrete. The shear capacity of the tested MSFRPC beams using the RILEM equations are shown in **Figure 19**. Comparison of test results and predictions shows that the shear capacities of all the test specimens were conservatively estimated.

6.2 Shear Predictions using Fib-Model Code2010 Provisions (fib-MC2010)

Fib-MC2010 code [61] explicitly includes several parameters in the shear capacity calculations ($V_{\mathrm{Rd,F}}$). The parameters included in Fib-MC2010 for shear estimations include: (i) reinforcement

ratio of longitudinal bars (ρ_l), (ii) size effect factor which accounts the size influence on shear capacity of beam (K), (iii) concrete compressive strength (f_{ck}), (iv) average prestressing stress acting on the cross-section of concrete due to prestressing action (σ_{cp}), (v) fracture parameters such as ultimate residual tensile strength (f_{Ftuk}) and characteristic value of tensile strength of concrete matrix (f_{ctk}). The residual tensile strength of FRC was calculated at the CMODs of 0.5 mm and 2.5 mm. Based on the experimentally observed fracture test results (f_{R1} and f_{R3}), the residual tensile capacities (f_{Ftuk}) of different fibre dosages were calculated using the equations shown in **Table 8**. In these calculations, the partial safety factor of the concrete material is considered as 1. The obtained shear capacity of MSFRPC beams is shown in **Figure 19**.

Table 8. Shear capacity equations of RILEM recommendations and Fib-MC2010 provisions

Code	Capacity (V)	Theoretical Shear Capacity Formulas
RILEM	Concrete (V_{cd})	$V_{cd} = \left[0.12\ k\ (100\ \rho_l f_{ck})^{\frac{1}{3}} + 0.15\sigma_{cp}\right] b\ d,\ k_l = k = 1 + \sqrt{\frac{200}{d}} \leq 2$ $k_f = 1 + \mathrm{n}\left(\frac{h_f}{b_w}\right)\left(\frac{h_f}{d}\right) \leq 1.5\ ,n = \left(\frac{b_f - b_w}{h_f}\right) \leq 3\ ,\ \rho_l = \frac{A_s}{bd} \leq 0.002$
	Fibres (V_{fd})	$V_{fd} = 0.7\ k_f k_l\ \tau_{fd}\ b\ d,\ \tau_{fd} = 0.12\ f_{RK,4}$
	Prestress (σ_{cp})	$\sigma_{cp} = \left(\frac{N_{sd}}{A_c}\right)$
Fib-MC2010	Concrete ($V_{\mathrm{Rd,F}}$)	$V_{Rd,F} = \left\{0.18\ K\left[100\ \rho_l\ \left(1 + 7.5\ \frac{f_{\mathrm{Ftuk}}}{f_{\mathrm{ctk}}}\right) f_{\mathrm{ck}}\right] + 0.15\ \sigma_{\mathrm{cp}}\right\}^{1/3} b_{\mathrm{w}}\ d$
		$f_{\mathrm{Ftu}}(w_{\mathrm{u}}) = f_{\mathrm{Fts}} - \frac{w_{\mathrm{u}}}{2.5}(f_{\mathrm{Fts}} - 0.5\ f_{\mathrm{R3}} + 0.2\ f_{\mathrm{R1}}) \geq 0$
		$f_{\mathrm{Fts}} = 0.45 f_{\mathrm{R1}},\ f_{\mathrm{ck}} = f_{\mathrm{cm}} - 8\ ,\ f_{\mathrm{ctm}} = 0.3 {f_{\mathrm{ck}}}^{2/3}$
	Prestress (σ_{cp})	$\sigma_{cp} = \left(\frac{N_{sd}}{A_c}\right)$

The ratio of experimental to theoretically calculated shear capacity of MSFRPC beams is 1.5, 1.7, 1.5, and 1.5 for MSF00, MSF50, MSF100, and MSF150, respectively. The prediction comparison of fib-MC2010, RILEM, and FEM predictions show that the FEM results closely predict the test results than the existing code provisions (**Figure 19)**. Not many studies have focused on the performance improvement of prestressed concrete beams under shear through macro synthetic fibre addition. More experimental research on macro-synthetic fibre reinforced concrete beams under shear loads for a wide range of parameters is required to develop a rational shear capacity model for design purposes. It is a scope for future work.

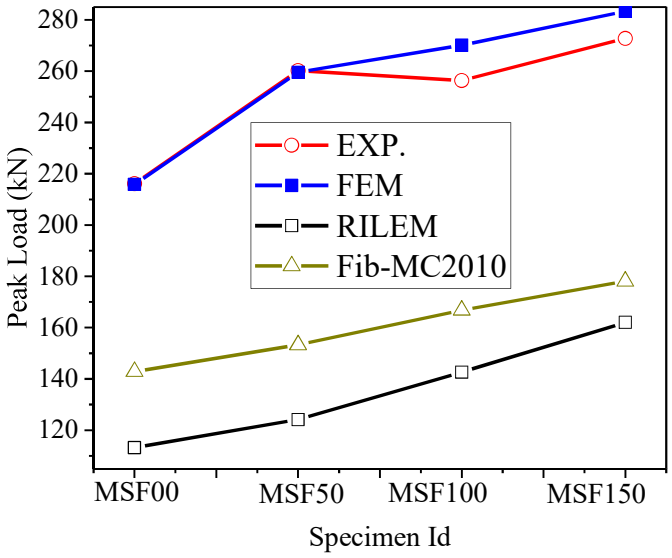

Figure 19. Comparison of shear capacity predictions with experimental and FEM predictions

7.0 SUMMARY AND CONCLUSIONS

The shear behaviour of MSFPRC concrete beams was studied through experimental and numerical means. The effect of volume fraction of macro synthetic fibres was considered. Tension stress-strain response of macro synthetic FRC obtained from the inverse analysis was used as input for FEM analysis. The nonlinear three-dimensional finite element models were developed, and the

predictions were validated with test results. The load-deflection response and failure modes were compared with FEM results. After that, a detailed parametric study was performed by varying the level of prestressing. Based on this limited study, the following conclusions can be drawn:

1. The fracture test results revealed that the macro synthetic fibres are effective at higher crack opening displacements higher than 2.5mm. Due to addition of macro synthetic fibers of 1.0% and 1.5% of volume fractions, the fracture energy increased by 9.6 and 16 times compared to control specimen.
2. The failure mode of prestressed concrete beams changed from brittle to ductile mode due to the addition of fibres at 0.5%, 1%, and 1.5%. The energy absorption capacity increased by 3.7, 4 and 6 times for 0.5%, 1.0% and 1.5% volume of fibre addition.
3. The predictions of load-deflection and failure mode using the finite element approach adopted in this study closely matched the test results. Parametric studies showed that the shear capacity of prestressed concrete beams increased by up to 18 % with an increase in fibre dosage and up to 15% due to increase in level of prestressing.
4. The shear capacity estimations by RILEM and fib-MC2010 code predictions are very conservative compared to FE predictions. More research is required on macro-synthetic fiber reinforced concrete beams to improve the existing code provisions.

8.0 ACKNOWLEDGEMENTS

The authors would like to acknowledge the financial support from the Ministry of Tribal Affairs India through Award No: 201920-NFST-TEL-01354, Utchattar Avishkar Yojana (UAY) Scheme, Government of India through Grant No: UAY-IITH_008, and PRECA India Pvt. Ltd. for

sponsoring the materials required for this research. Specimens were cast at the precast yard of PRECA India Pvt. Ltd.

9.0 CONFLICTS OF INTEREST

None.

10.0 DATA AVAILABILITY STATEMENT

Some or all data and models that support the findings of this study are available from the corresponding author upon reasonable request.

11.0 REFERENCES

[1] B.A. Graybeal, Flexural behavior of an ultrahigh-performance concrete I-girder, J. Bridg. Eng. 13 (2008) 602–610. https://doi.org/10.1061/(ASCE)1084-0702(2008)13:6(602).

[2] D.B. Garber, J.M. Gallardo, D.J. Deschenes, O. Bayrak, Nontraditional Shear Failures in Bulb-T Prestressed Concrete Bridge Girders, J. Bridg. Eng. 21 (2016) 1–10. https://doi.org/10.1061/(ASCE)BE.1943-5592.0000890.

[3] G.P. Osborn, P.J. Barr, D.A. Petty, M.W. Halling, T.R. Brackus, Residual prestress forces and shear capacity of salvaged prestressed concrete bridge girders, J. Bridg. Eng. 17 (2012) 302–309. https://doi.org/10.1061/(ASCE)BE.1943-5592.0000212.

[4] K.H. Tan, F.K. Kong, L.W. Weng, High-strength reinforced concrete deep and short beams: Shear design equations in North American and UK practice, ACI Struct. J. 95 (1998) 318–329. https://doi.org/10.14359/549.

[5] W. Ji, W. Li, M. An, L. Zhu, Shear Capacity of T-Section Girders Made of Reactive Powder

Concrete, J. Bridg. Eng. 23 (2018) 1–20. https://doi.org/10.1061/(ASCE)BE.1943-5592.0001253.

[6] S.J. Hwang, W.Y. Lu, H.J. Lee, Shear strength prediction for deep beams, ACI Struct. J. 97 (2000) 367–376. https://doi.org/10.14359/9624.

[7] Y. Chi, M. Yu, L. Huang, L. Xu, Finite element modeling of steel-polypropylene hybrid fiber reinforced concrete using modified concrete damaged plasticity, Eng. Struct. 148 (2017) 23–35. https://doi.org/10.1016/j.engstruct.2017.06.039.

[8] S. Gali, K.V.L. Subramaniam, Shear behavior of slender and non-slender steel fiber-reinforced concrete beams, ACI Struct. J. 116 (2019) 149–158. https://doi.org/10.14359/51713307.

[9] S.J. Foster, A. Agarwal, A. Amin, Design of steel fiber reinforced concrete beams for shear using inverse analysis for determination of residual tensile strength, Struct. Concr. 19 (2018) 129–140. https://doi.org/10.1002/suco.201700100.

[10] D.R. Sahoo, A. Solanki, A. Kumar, Influence of steel and polypropylene fibers on flexural behavior of RC beams, J. Mater. Civ. Eng. 27 (2015) 1–9. https://doi.org/10.1061/(ASCE)MT.1943-5533.0001193.

[11] W. Kaufmann, A. Amin, A. Beck, M. Lee, Shear transfer across cracks in steel fibre reinforced concrete, Eng. Struct. 186 (2019) 508–524. https://doi.org/10.1016/j.engstruct.2019.02.027.

[12] A. Amin, S.J. Foster, Shear strength of steel fibre reinforced concrete beams with stirrups, Eng. Struct. 111 (2016) 323–332. https://doi.org/10.1016/j.engstruct.2015.12.026.

[13] A. Dev, M. Chellapandian, S.S. Prakash, Effect of Macrosynthetic and Hybrid Fibers on Shear Behavior of Concrete Beams Reinforced with GFRP Bars, J. Bridg. Eng. 25 (2020)

1–16. https://doi.org/10.1061/(ASCE)BE.1943-5592.0001557.

[14] J.A. McMahon, A.C. Birely, Experimental Performance of Steel Fiber Reinforced Concrete Bridge Deck, J. Bridg. Eng. 23 (2018) 1–14. https://doi.org/10.1061/(ASCE)BE.1943-5592.0001287.

[15] E. Cuenca, P. Serna, Shear behavior of prestressed precast beams made of self-compacting fiber reinforced concrete, Constr. Build. Mater. 45 (2013) 145–156. https://doi.org/10.1016/j.conbuildmat.2013.03.096.

[16] ACI Committee 318, Building Code Requirements Available for Public Review (ACI 318-19), 2019.

[17] J.S. Cho, J. Lundy, S.H. Chao, Shear strength of steel fiber reinforced prestressed concrete beams, Proc. 2009 Struct. Congr. - Don't Mess with Struct. Eng. Expand. Our Role. (2009) 1058–1066. https://doi.org/10.1061/41031(341)117.

[18] C. Lakavath, S.S. Joshi, S.S. Prakash, Investigation of the effect of steel fibers on the shear crack-opening and crack-slip behavior of prestressed concrete beams using digital image correlation, Eng. Struct. 193 (2019) 28–42. https://doi.org/10.1016/J.ENGSTRUCT.2019.05.030.

[19] M.A. Rasheed, S.S. Prakash, Behavior of hybrid-synthetic fiber reinforced cellular lightweight concrete under uniaxial tension – Experimental and analytical studies, Constr. Build. Mater. 162 (2018) 857–870. https://doi.org/10.1016/j.conbuildmat.2017.12.095.

[20] M.A. Rasheed, S.S. Prakash, Mechanical behavior of sustainable hybrid-synthetic fiber reinforced cellular light weight concrete for structural applications of masonry, Constr. Build. Mater. 98 (2015) 631–640. https://doi.org/10.1016/j.conbuildmat.2015.08.137.

[21] A. Bhosale, M.A. Rasheed, S.S. Prakash, G. Raju, A study on the efficiency of steel vs.

synthetic vs. hybrid fibers on fracture behavior of concrete in flexure using acoustic emission, Constr. Build. Mater. 199 (2019) 256–268. https://doi.org/10.1016/j.conbuildmat.2018.12.011.

[22] A. Conforti, F. Minelli, A. Tinini, G.A. Plizzari, Influence of polypropylene fibre reinforcement and width-to-effective depth ratio in wide-shallow beams, Eng. Struct. 88 (2015) 12–21. https://doi.org/10.1016/j.engstruct.2015.01.037.

[23] M.N. Soutsos, T.T. Le, A.P. Lampropoulos, Flexural performance of fibre reinforced concrete made with steel and synthetic fibres, Constr. Build. Mater. 36 (2012) 704–710. https://doi.org/10.1016/j.conbuildmat.2012.06.042.

[24] B. Boulekbache, M. Hamrat, M. Chemrouk, S. Amziane, Influence of yield stress and compressive strength on direct shear behaviour of steel fibre-reinforced concrete, Constr. Build. Mater. 27 (2012) 6–14. https://doi.org/10.1016/j.conbuildmat.2011.07.015.

[25] N. Buratti, C. Mazzotti, M. Savoia, Post-cracking behaviour of steel and macro-synthetic fibre-reinforced concretes, Constr. Build. Mater. 25 (2011) 2713–2722. https://doi.org/10.1016/j.conbuildmat.2010.12.022.

[26] Y. Chi, L. Xu, H. sui Yu, Constitutive modeling of steel-polypropylene hybrid fiber reinforced concrete using a non-associated plasticity and its numerical implementation, Compos. Struct. 111 (2014) 497–509. https://doi.org/10.1016/j.compstruct.2014.01.025.

[27] J. Lee, G.L. Fenves, ASCE, Plastic-Damage Model for Cyclic Loading of Concrete Structures, J. Eng. Mech. 124 (1998) 892–900.

[28] J. Lubliner, J. Oliver, S. Oller, E. Onate, a Plastic-Damage Model, Int. J. Solids Struct. 25 (1989) 299–326.

[29] S.J. Stephen, B. Raphael, R. Gettu, S. Jose, Determination of the tensile constitutive

relations of fiber reinforced concrete using inverse analysis, Constr. Build. Mater. 195 (2019) 405–414. https://doi.org/10.1016/j.conbuildmat.2018.11.014.

[30] G. Kani, How Safe are Our Large Reinforced Concrete Beams?, ACI J. Proc. 64 (1967). https://doi.org/10.14359/7549.

[31] M. Shahnewaz, M.S. Alam, Improved shear equations for steel fiber-reinforced concrete deep and slender beams, ACI Struct. J. 111 (2014) 851–860. https://doi.org/10.14359/51686736.

[32] B.I. Mihaylov, J. Liu, K. Simionopoulos, E.C. Bentz, M.P. Collins, Effect of member size and tendon layout on shear behavior of post-tensioned beams, ACI Struct. J. 116 (2019) 265–274. https://doi.org/10.14359/51715633.

[33] Bureau of Indian Standards, IS 10262- 2019, Concrete mix proportioning- guidelines, (2019) 1–40.

[34] A. Enfedaque, M.G. Alberti, J.C. Gálvez, Influence of fiber distribution and orientation in the fracture behavior of polyolefin fiber-reinforced concrete, Materials (Basel). 12 (2019). https://doi.org/10.3390/ma12020220.

[35] S.T. Kang, J.K. Kim, The relation between fiber orientation and tensile behavior in an ultra high performance fiber reinforced cementitious composites (UHPFRCC), Cem. Concr. Res. 41 (2011) 1001–1014. https://doi.org/10.1016/j.cemconres.2011.05.009.

[36] F. Laranjeira, A. Aguado, C. Molins, S. Grünewald, J. Walraven, S. Cavalaro, Framework to predict the orientation of fibers in FRC: A novel philosophy, Cem. Concr. Res. 42 (2012) 752–768. https://doi.org/10.1016/j.cemconres.2012.02.013.

[37] A. Abrishambaf, M. Pimentel, S. Nunes, Influence of fibre orientation on the tensile behaviour of ultra-high performance fibre reinforced cementitious composites, Cem. Concr.

Res. 97 (2017) 28–40. https://doi.org/10.1016/j.cemconres.2017.03.007.

[38] F.Y. Li, L.Y. Li, Y. Dang, P.F. Wu, Study of the effect of fibre orientation on artificially directed steel fibre-reinforced concrete, Adv. Mater. Sci. Eng. 2018 (2018). https://doi.org/10.1155/2018/8657083.

[39] F. Laranjeira, S. Grünewald, J. Walraven, C. Blom, C. Molins, A. Aguado, Characterization of the orientation profile of steel fiber reinforced concrete, Mater. Struct. Constr. 44 (2011) 1093–1111. https://doi.org/10.1617/s11527-010-9686-5.

[40] I. Şanal, N. Özyurt Zihnioğlu, To what extent does the fiber orientation affect mechanical performance?, Constr. Build. Mater. 44 (2013) 671–681. https://doi.org/10.1016/j.conbuildmat.2013.03.079.

[41] G. Srikar, G. Anand, S.S. Prakash, A Study on Residual Compression Behavior of Structural Fiber Reinforced Concrete Exposed to Moderate Temperature Using Digital Image Correlation, Int. J. Concr. Struct. Mater. 10 (2016) 75–85. https://doi.org/10.1007/s40069-016-0127-x.

[42] A.B. Bhosale, C. Lakavath, S. Suriya Prakash, Multi-linear tensile stress-crack width relationships for hybrid fibre reinforced concrete using inverse analysis and digital image correlation, Eng. Struct. 225 (2020) 111275. https://doi.org/10.1016/j.engstruct.2020.111275.

[43] L. Vandewalle, D. Nemegeer, G.L. Balazs, B. Barr, P. Bartos, N. Banthia, A.M. Brandt, M. Criswell, F. Denarie, M. di Prisco, H. Falkner, R. Gettu, V. Gopalaratnam, P. Groth, V. Hausler, F. Katsaragafis, A. Kooiman, K. Kovler, J. Lehtonen, B. Massicotte, S. Mindess, H. Reinhardt, P. Rossi, S. Schaerlaekens, B. Schnutgen, S. Shah, A. Skarendahl, H. Stang, P. Stroeven, R. Swamy, P. Tatnall, M. Teutsch, J. Walraven, A. Wubs, Rilem TC 162-TDF:

Test and design methods for steel fibre reinforced concrete: Uni-axial tension test for steel fibre reinforced concrete, Mater. Struct. Constr. 34 (2001) 3–6. https://doi.org/10.1617/13628.

[44] JCI-S-002-2003, Method of test for load-displacement curve of fiber reinforced concrete by use of notched beam, (2003) 3–8.

[45] ASTM International., 1061/A1061M-09 Standard Test Methods for Testing Multi-Wire Steel Strand., West Conshohocken, PA; ASTM Int. (2009). https://doi.org/https://doi.org/10.1520/A1061_A1061M-09.

[46] A. Thorenfeldt, E. Tomaszewicz, J.J. Jensen, Mechanical Properties of High-strengthConcrete and Application in Design, in: Proc. Symp. Util. High-StrengthConcrete, Tapir, Trondheim, 1987: pp. 149–159.

[47] Y.C. Ou, M. Sen Tsai, K.Y. Liu, K.C. Chang, Compressive Behavior of Steel-Fiber-Reinforced Concrete with a High Reinforcing Index, J. Mater. Civ. Eng. 24 (2012) 207–215. https://doi.org/10.1061/(ASCE)MT.1943-5533.0000372.

[48] Z. Huang, J.Y.R. Liew, Nonlinear finite element modelling and parametric study of curved steel-concrete-steel double skin composite panels infilled with ultra-lightweight cement composite, Constr. Build. Mater. 95 (2015) 922–938. https://doi.org/10.1016/j.conbuildmat.2015.07.134.

[49] JCI-S-001-2003, Method of test for fracture energy of concrete by use of notched beam, 2 (2003) 1–14.

[50] T. Yu, J.G. Teng, Y.L. Wong, S.L. Dong, Finite element modeling of confined concrete-II: Plastic-damage model, Eng. Struct. 32 (2010) 680–691. https://doi.org/10.1016/j.engstruct.2009.11.013.

[51] Y. Chi, L. Xu, H.S. Yu, Plasticity model for hybrid fiber-reinforced concrete under true triaxial compression, J. Eng. Mech. 140 (2014) 393–405. https://doi.org/10.1061/(ASCE)EM.1943-7889.0000659.

[52] C. Lakavath, M.S.V. Sagi, S.S. Joshi, S.S. Prakash, Finite element studies on the flexure-shear behavior of steel and hybrid fiber reinforced prestressed concrete beams, Indian Concr. J. 95 (2021) 58–70.

[53] Abaqus 6.11, Abaqus 6.11. Dassault Systemes Simulia Corp Providence, (2011).

[54] T. Rahman, W. Lutz, R. Finn, S. Schmauder, S. Aicher, Simulation of the mechanical behavior and damage in components made of strain softening cellulose fiber reinforced gypsum materials, Comput. Mater. Sci. 39 (2007) 65–74. https://doi.org/10.1016/j.commatsci.2006.01.032.

[55] A.S. Genikomsou, M.A. Polak, Finite element analysis of punching shear of concrete slabs using damaged plasticity model in ABAQUS, Eng. Struct. 98 (2015) 38–48. https://doi.org/10.1016/j.engstruct.2015.04.016.

[56] A. Wosatko, A. Winnicki, M.A. Polak, J. Pamin, Role of dilatancy angle in plasticity-based models of concrete, Arch. Civ. Mech. Eng. 19 (2019) 1268–1283. https://doi.org/10.1016/j.acme.2019.07.003.

[57] M. Lapi, L. Secci, E. Teoni, A.P. Ramos, M. Orlando, A hybrid method for the calibration of finite element models of punching-shear in R/C flat slabs, Comput. Struct. 238 (2020) 106323. https://doi.org/10.1016/j.compstruc.2020.106323.

[58] A. Earij, G. Alfano, K. Cashell, X. Zhou, Nonlinear three–dimensional finite–element modelling of reinforced–concrete beams: Computational challenges and experimental validation, Eng. Fail. Anal. 82 (2017) 92–115.

https://doi.org/10.1016/j.engfailanal.2017.08.025.

[59] J.G. Stoner, Finite Element Modelling of GFRP Reinforced, University of Waterloo, 2015.

[60] A.A. Arab, S.S. Badie, M. T., A methodological approach for finite element modeling of pretensioned concrete members at the release of pretensioning, Eng. Struct. 33 (2011) 1918–1929. https://doi.org/10.1016/j.engstruct.2011.02.028.

[61] Model Code 2010-First complete draft-Volume 2: Model Code. Vol. 56., Fédération Internationale du Béton (fib), 2010.